Spreading dynamics of power-law fluid droplets

2009 J. Phys.: Condens. Matter 21 464117

(http://iopscience.iop.org/0953-8984/21/46/464117)

J. Phys.: Condens. Matter **21** (2009) 464117 (10pp) doi:10.1088/0953-8984/21/46/464117

Spreading dynamics of power-law fluid droplets

Zhan-Peng Liang[1], Xiao-Dong Wang[2], Duu-Jong Lee[3,5], Xiao-Feng Peng[1] and Ay Su[4]

[1] Lab of Phase Change and Interfacial Transport Phenomena, Department of Thermal Engineering, Tsinghua University, Beijing 100084, People's Republic of China
[2] Department of Thermal Engineering, School of Mechanical Engineering, University of Science and Technology Beijing, Beijing 100083, People's Republic of China
[3] Department of Chemical Engineering, National Taiwan University, Taipei 106, Taiwan
[4] Department of Mechanical Engineering, Fuel Cell Center, Yuan Ze University, Taoyuan 300, Taiwan

E-mail: djlee@ntu.edu.tw

Received 15 April 2009, in final form 30 April 2009
Published 29 October 2009
Online at stacks.iop.org/JPhysCM/21/464117

Abstract
This paper aims at providing a summary of the theoretical models available for non-Newtonian fluid spreading dynamics. Experimental findings and model predictions for a Newtonian fluid spreading test are briefly reviewed. Then how the complete wetting and partial wetting power-law fluids spread over a solid substrate is examined. The possible extension of Newtonian fluid models to power-law fluids is also discussed.

(Some figures in this article are in colour only in the electronic version)

1. Introduction

Wetting solid surfaces using liquids has broad applications in printing, painting, adhesion, lubrication, and spraying. Figure 1 (upper panel) depicts schematically the drop wetting process. Extensive studies have been devoted to spreading and wetting dynamics of Newtonian fluids. In particular, ways of removing the stress singularity in the immediate region of the contact line were proposed. Pertinent review articles on wetting and spreading of fluids are available in de Gennes [1], Leger and Joanny [2], Voinov [3], Blake [4], and in the books by Berg [3], de Gennes *et al* [5], and Starov *et al* [6].

Numerous polymer solutions and particulate suspensions exhibit non-Newtonian characteristics. Only a few theoretical and experimental studies have explored how non-Newtonian fluids spread over solid substrates [7–14]. In this paper, the experimental observations and theoretical models for spreading and wetting of Newtonian fluids are briefly reviewed (section 2). Both complete wetting and partial wetting systems are discussed. Then, the lubrication models available in open literature for power-law fluids are summarized (section 3). The possible extension of Newtonian fluid models to power-law fluids is discussed.

[5] Author to whom any correspondence should be addressed.

2. Spreading and wetting of Newtonian fluids

2.1. Experimental observation

For a drop of a complete wetting fluid with radius smaller than the capillary length, $l_c = \sqrt{\sigma/\rho g}$, the drop can spread until it reaches a film thickness controlled by surface forces. For thin droplets with radius $R(t)$, $-h'(R) = \tan(\theta_{ap}) \approx \theta_{ap}$, where θ_{ap} is the apparent contact angle, and $\theta_{ap} \propto R(t)^{-3}$, assuming the drop has a spherical shape.

Correlations between contact angle and the droplet spreading speed were developed. For complete wetting of small drops, the well known Tanner's law was applied [15]:

$$R(t) \propto t^m. \tag{1}$$

The power $m = 1/10$ is noted for viscous spreading of small droplets [16]. As the radius of the droplet grows beyond the capillary length, the gravity force dominates and the shape of the drop becomes pancake-like, curved only at the drop rim, yielding an $m = 1/8$ when bulk phase fluid dissipation dominates or $m = 1/7$ when contact line fluid dissipation dominates [17]. A crossover between $m = 1/10$ and $1/8$ was reported in the experiments of Cazabat and Cohen-Stuart [18], while Ehrhard [19] found a crossover from $1/10$ to $1/7$.

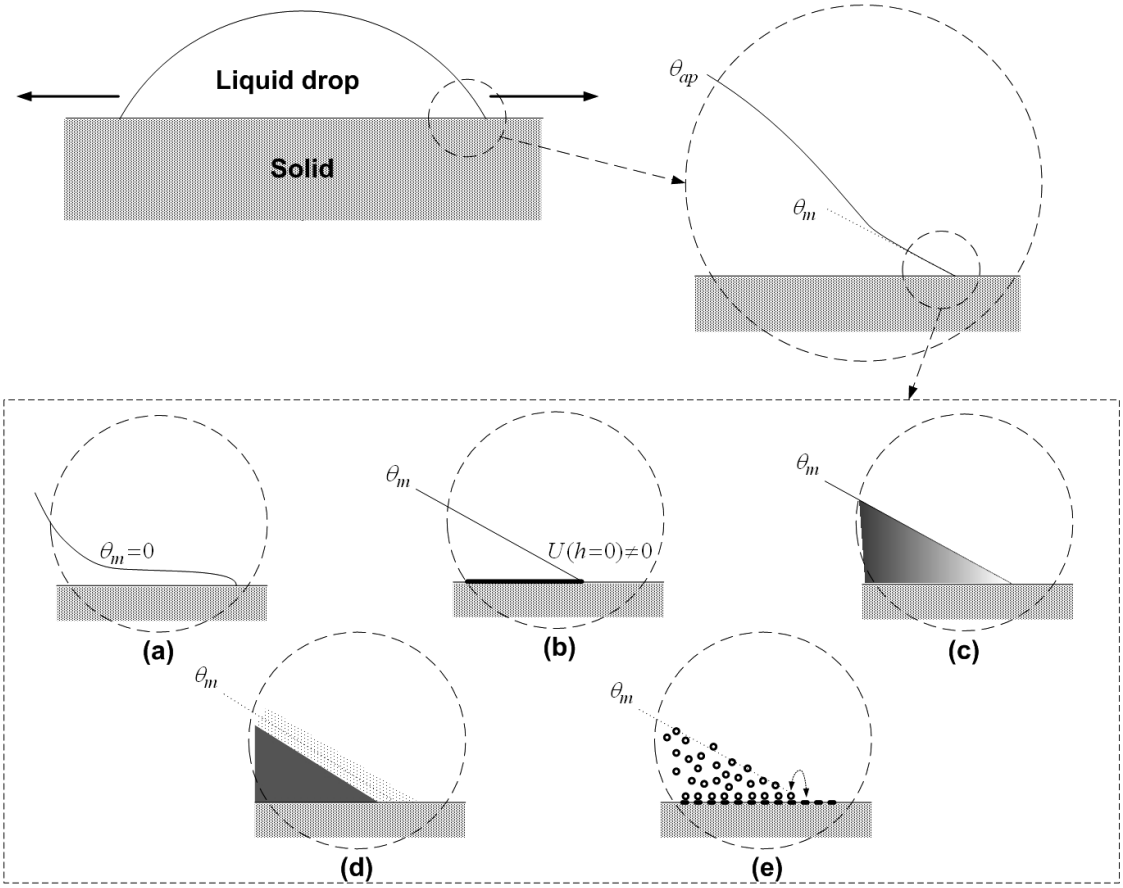

Figure 1. Schematic diagram of a spreading drop and various mechanisms proposed for relieving the dynamic singularity at the moving contact line. (a) Precursor film; (b) velocity slip at the wall; (c) shear-thinning transition; (d) diffuse interface; (e) molecular hopping process.

Viscous dissipation in drop spreading for low viscosities is negligible, which leads to $m = 1/2$ in the early stage of wetting [20], and $m = 2/3$ in the latter stage of wetting [21].

Much less information is known for partial wetting fluid spreading. Lavi and Marmur [22] proposed the following equation for correlating the spreading data for Newtonian fluids:

$$A = A_{\mathrm{eq}}\left(1 - \exp\left(-\frac{a}{A_{\mathrm{eq}}}t^m\right)\right) \tag{2}$$

where A is the wet area of the spreading droplet, and a and m are coefficients.

2.2. Theoretical models

Use of Navier–Stokes equations for describing the spreading of Newtonian fluids with the no-slip boundary condition yields a diverging energy dissipation rate at the contact line [23]. At least five approaches have been adopted to overcome the stress singularity difficulty.

A conventional view for the complete wetting fluids considers the contact line to be preceded by a thin fluid precursor film, which is driven by van der Waals forces [1, 24, 25]. The precursor film at a thickness of 10–100 nm has been experimentally confirmed [26–28] (figure 1(a), lower panel).

A slip boundary at the contact line was adopted to remove the stress singularity paradox [23, 29, 30], which was later verified by MD simulations [31, 32]. Recently, Thompson and Troian proposed a generalized slip boundary condition relating to the static properties and dynamic interactions of the walls and the fluid [33] (figure 1(b), lower panel).

The stress singularity would vanish if the fluids exhibited shear-thinning properties [34–36]. The viscosity of shear-thinning fluids decreases as shear rate grows, so the entire viscous dissipation rate is finite (figure 1(c), lower panel).

The chemical-potential-gradient-induced diffusion interprets the motion of the contact line in the framework of the diffuse-interface model [37–42]. The diffuse-interface model assumes an interface of finite thickness over which various properties change continuously (figure 1(d), lower panel). A similar model has been developed by Shikhmurzaev, which focused on a third interface phase with its own properties [43–45].

Blake and his co-workers developed a model accounting for the unequal frequencies of liquid molecules hopping across the contact line at the solid surface [46–48]. This model is referred to as the 'molecular kinetic theory' (MKT), and assumes that energy dissipation occurs in the immediate vicinity of the moving contact line due to the adsorption and desorption process of fluid particles on the adsorption sites at the solid surface [49] (figure 1(b), lower panel).

Although most studies on fluid spreading or wetting are based on the lubrication approximation without inertial components, recent articles [50–52] have considered inertia force in Newtonian fluid spreading. The inertia components decrease the interface deformation and the apparent contact angle compared to the case with $Re = 0$ at the same capillary number ($Ca = U\mu/\sigma$).

3. Models for non-Newtonian fluids

3.1. Fluid rheology and experiments

Research on non-Newtonian fluid spreading considered shear-thinning fluids [7–14, 34, 35, 53–55], shear-thickening fluids [8–10, 13, 14] or viscoelastic fluids [11, 12, 54, 56]. For shear-thinning or shear-thickening liquids, namely the power-law liquids, the constitutive relationship can be expressed as follows:

$$\tau = k\dot{\gamma}^n \tag{3}$$

$$\mu = k\dot{\gamma}^{n-1} \tag{4}$$

where τ denotes the shear force, $\dot{\gamma}$ denotes the shear rate, k denotes the consistency coefficient, n denotes the power exponent and μ the apparent viscosity, respectively. If $n < 1$, the apparent viscosity decreases as the shear rate increases, revealing a shear-thinning characteristic. At $n > 1$, the apparent viscosity increases as the shear rate increases, and the fluids are shear-thickening or dilatant fluids. At $n = 1$, equations (3) and (4) converge to a Newtonian fluid.

For fluids with normal stress effects, the Reiner–Rivlin expression is adopted:

$$\vec{\tau} = 2\mu\dot{E} + \alpha\dot{E}\cdot\dot{E} \tag{5}$$

where μ and α are constant coefficients related to fluid properties and $\dot{E}$ is the shear rate tensor; in this case $\dot{E} = 1/2\partial v_x/\partial z(\vec{e}_x\vec{e}_z + \vec{e}_z\vec{e}_x)$. The stress components which are not zero are the shear stress, $\tau_{zx} = \mu(\frac{\partial v_x}{\partial z})$, and the normal stress, $\tau_{xx} = \tau_{zz} = \frac{\alpha}{4}(\frac{\partial v_x}{\partial z})^2$.

We compared the theoretical models in the next sections with the spreading data collected in the literature and with those collected in this study. An experimental section is available in the appendix. Also, we noted dynamic surface tension effects for the commonly used xanthan solutions, which should be considered in experimental design and subsequent data analysis.

3.2. Lubrication models

Most theoretical models for non-Newtonian spreading adopted the lubrication approximation and no-slip boundary conditions at the contact line regime (figure 2). One group of researchers assumed a wedge shaped contact line surface [7, 54] (figure 1(b)), and another group of researchers assumed a free surface [8–10, 13, 55]. These models consider a two-dimensional spreading at a steady velocity of U using a Cartesian coordinate framework.

The lubrication approximation form of the flow equation can be stated as follows:

$$\frac{\partial p}{\partial x} = \frac{\partial}{\partial y}\left(\mu\frac{\partial u}{\partial y}\right). \tag{6}$$

The boundary conditions consist of the no-slip condition at the solid surface and the no-shear condition at the free surface:

$$u|_{z=0} = 0 \tag{7}$$

$$\left.\frac{\partial u}{\partial z}\right|_{z=h} = 0. \tag{8}$$

Integrating equation (6) along the z direction yields the velocity equation involving the pressure gradient in the x direction p_x and the thickness of the fluid layer h.

References [7, 54] adopted a wedge-like layer at the contact line regime as follows:

$$h = \theta x \tag{9}$$

where θ is the dynamic contact angle. Then integrating again the velocity equation along the z direction and substituting into the volume conservation equation leads to

$$Q = Uh \tag{10}$$

where Q is the volume flux across a layer section. One can hence obtain the explicit velocity distribution $u = u(x, h)$ [7], or its approximate expression [54].

We integrate the viscous dissipation in the flow region as follows:

$$E_v = \int_0^L \int_0^h \mu\left(\frac{\partial u}{\partial z}\right)^2 \mathrm{d}z\,\mathrm{d}x \tag{11}$$

where L is the macroscopic characteristic length of the wetting system, conventionally considered as the drop radius [1]. The energy balance of the wedge shape model takes a contact angle with the surface tension energy equilibrating with the viscous effect [1]:

$$E_v = E_\sigma = U\sigma(\cos\theta_{eq} - \cos\theta). \tag{12}$$

Equation (12) can be rearranged into the θ versus U relationship. Note that the developed wedge shape models account for capillary energy, hence are valid in the capillary wetting regime only.

Free surface models [8–10, 13, 55] followed a similar solution logic but released the wedge shape constraint for the contact line regime. Instead, these models looked for film thickness distribution by solving the stress balance equation. The presence of gravity acts on the liquid film as follows:

$$\frac{\partial p}{\partial z} = -\rho g. \tag{13}$$

The force balance normal to the free surface follows the Young–Laplace equation and can be stated as in the following:

$$p|_{z=h} = p_g - \sigma\frac{\frac{\partial^2 h}{\partial x^2}}{\left(1 + \left(\frac{\partial h}{\partial x}\right)^2\right)^{3/2}} \approx p_g - \sigma\frac{\partial^2 h}{\partial x^2} \tag{14}$$

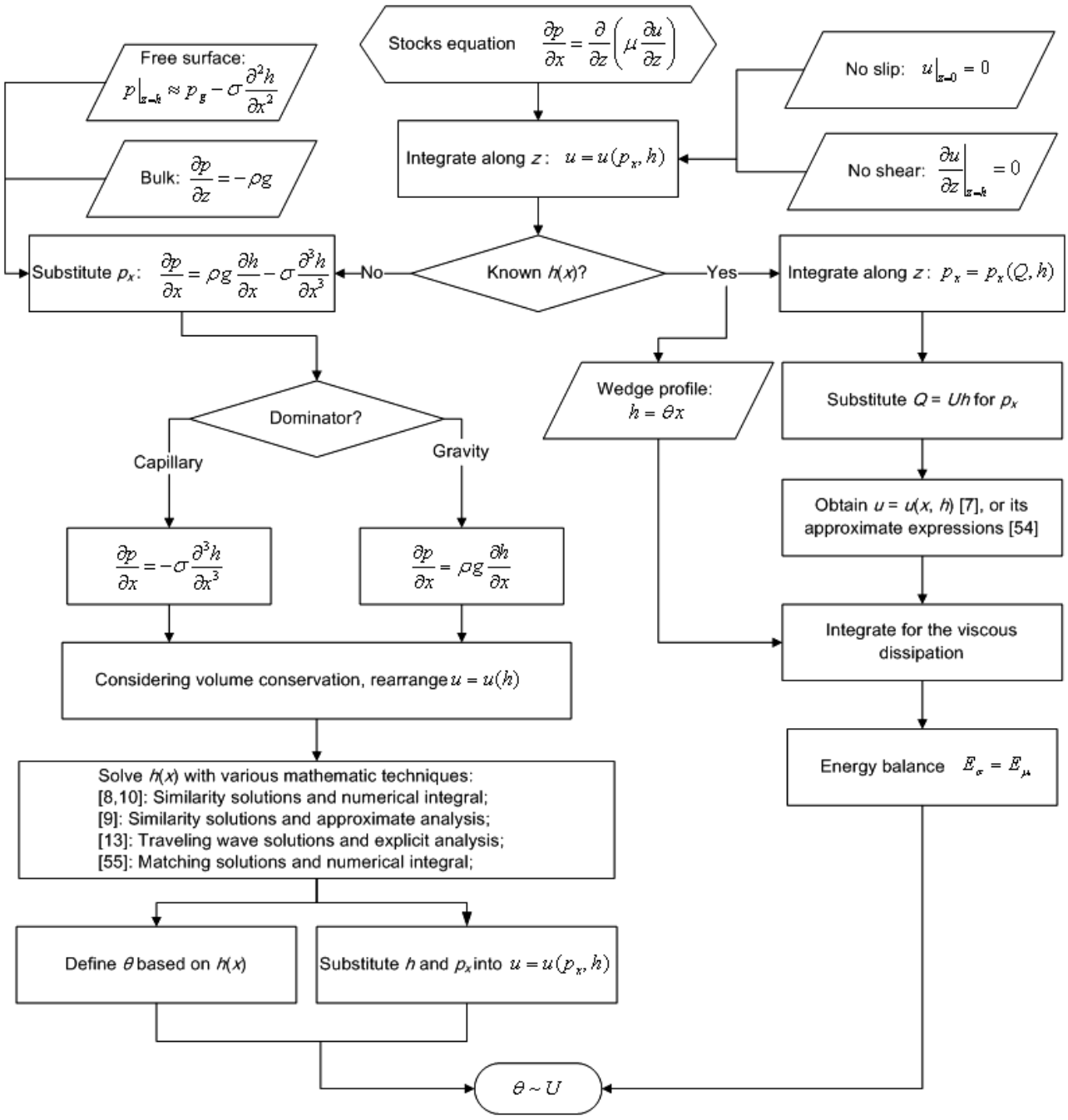

Figure 2. Schematic solution diagram of prevalent spreading models for non-Newtonian fluids.

where p_g is atmospheric pressure. Combining equations (13) and (14) yields

$$\frac{\partial p}{\partial x}=\rho g\frac{\partial h}{\partial x}-\sigma\frac{\partial^3 h}{\partial x^3}. \tag{15}$$

Substituting equation (15) into the volume conservation equation yields a partial differential equation for fluid layer thickness, $h(x)$. One can obtain analytical solutions for film thickness distributions considering the capillary wetting limit or gravitational wetting limit. The contact angle can thereby be defined and associated with the spreading speed U.

Starov *et al* [9] adopted the lubrication approximation to establish their hydrodynamic model for complete wetting, power-law fluids. Their derivation considering capillary force or gravity force dominated regimes for an approximate symmetrical sphere leads to respectively

$$R(t)\sim t^{\frac{n}{3n+5}} \tag{16}$$

or

$$R(t)\sim t^{\frac{n}{3n+7}}. \tag{17}$$

Betelu and Fontelos [8, 10] studied capillary spreading by adopting different self-similar solution forms from Starov *et al*, and solved the high-order ODE numerically without the assumption of complete wetting. These authors achieved exactly the same spreading laws (equations (16) and (17)) for

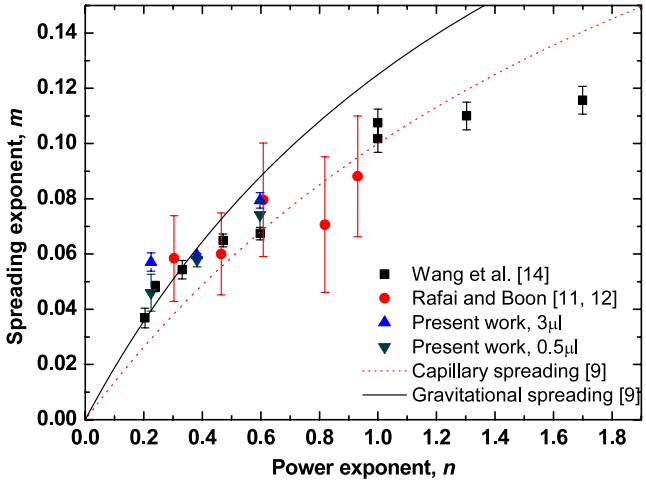

Figure 3. Comparison of spreading exponents of complete wetting fluids with Starov's model [9]. Solid curve, gravitational spreading curve; dotted curve, capillary spreading curve; squares, data of Wang *et al* [14]; solid circles, data of Rafai and Boon [11, 12]; triangles, data of present work.

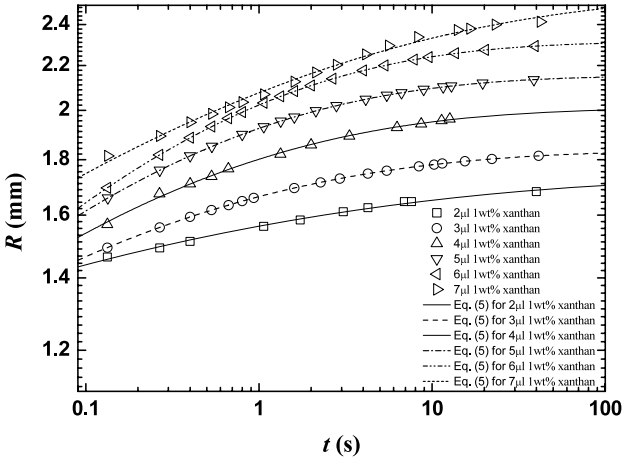

Figure 4. log $R(t)$–log t plot of 1 wt% xanthan solution with different droplet volumes.

the complete wetting fluids. Restated, in either the capillary or the gravity regime, the complete wetting shear-thinning fluid would spread more slowly than Newtonian fluids; conversely, the complete wetting shear-thickening fluids would spread faster than the Newtonian counterparts. At the $n \gg 1$ limit for the strongly shear-thickening characteristic, $R(t) \sim t^{1/3}$ for both capillary and gravity regimes. At the $n \to 0$ limit, for the strongly shear-thinning characteristic, $R(t) \sim t^{n/5}$ or $t^{n/7}$.

3.3. Spreading of complete wetting fluids

Wang *et al* [14] experimentally evaluated the spreading behavior for complete wetting and partial wetting power-law fluids. Their complete wetting data using five xanthan solutions with various concentrations on mica surface (shear-thinning fluids) and PPG + 7.5% w/w 10 nm silica powders and PPG + 10% w/w 10 nm silica on glass slides (shear-thickening fluids) are compared with those collected from Rafai *et al* [11, 12] in figure 3. The spreading data collected herein (see the appendix) are also included in the figure for comparison.

Experimental findings follow the same trend as noted for the prediction by Starov *et al* [9]: $m > 0.1$ when $n > 1$ and $m < 0.1$ when $n < 1$. At $n = 1, m = 0.1$, corresponding to the known Tanner's law (equation (1)) for capillary spreading for Newtonian fluids. However, certain deviations were noticeable between experimental data and the theory as n deviates from unity. As n decreases for shear-thinning fluids, the spreading index decreases, but the behavior gradually approaches the gravity controlled model. Particularly, when $n < 0.4$, the spreading well fitted the gravity spreading theory. Conversely, as n increases for shear-thickening fluids, the spreading index m is lower than those predicted by capillary or gravity models. For instance, at $n = 1.669$, $m = 0.1157 \pm 0.0045$, much lower than that predicted by capillary (0.140) or gravity (0.168) models. Carré and Woehl [36] interpreted that the Newtonian fluid will reveal the shear-thinning characteristic at high shear rate, such as at the contact line regime, to suppress the stress singularity in hydrodynamic modeling. The shear-thickening fluid reveals a flow characteristic similar to those with an apparent n (n_{app}) lower than that from the rheological test (n), as revealed in figure 3. For instance, at $n = 1.699$, n_{app} is only approximately 1.1 based on the Starov *et al* capillary model. One possible reason corresponding to the noted discrepancy is the limited diffusion rate for 10 nm silica powders in PEG suspension at the contact line regime when the dilatant fluid spreads. The contact line regime may be enriched by pure PPG liquid with a minimal quantity of silica powders, a Newtonian fluid behavior hence prevailing.

3.4. Partial wetting fluid spreading

de Ruijter *et al* [57] divided the spreading process into three stages: initial, $R(t) \approx R_0 + at$; and the intermediate stage; and finally, $R(t) \propto t^{0.1}$. Wang *et al* [14] refined the approach by Lavi and Marmur [22] using contact radius as the fitting parameter to correlate the spreading data of power-law fluids (equation (18)).

$$R = R_{eq}\left(1 - \exp\left(-\frac{a}{R_{eq}}t^m\right)\right). \tag{18}$$

For the completely wetting system, $R_{eq} \to \infty$, so equation (18) converges to $R = at^m$, the correlation for completely wetting systems. The parameters a and m were used as fitting parameters for linearly regressing $R(t)$ with known R_{eq}. The higher m corresponds to the faster drop spreading on the substrate.

The droplet volume affects the spreading dynamics for non-Newtonian fluids. Figure 4 shows the spreading radius of 1 wt% xanthan solution with different droplet volumes. The single power law $R = at^m$ fails to describe the entire data range, while the empirical equation, equation (18), describes well the data. Table 1 lists the regression parameters of each set of spreading data by equation (18). As the drop volume increases, the spreading exponent m increases, indicating that

Table 1. Best-fit parameters for partially wetting, power-law fluids and power exponents of equation (18).

Concentration (wt%)	Volume (μl)	R_{eq} (m)	a	m	θ_{eq} (deg)	Correlation coefficients r^2
1	2	0.001 682	0.004 365	0.1868	35.3	0.9955
	3	0.001 814	0.004 463	0.1909	35.1	0.9962
	4	0.001 964	0.004 650	0.2040	34.5	0.9977
	5	0.002 135	0.004 890	0.2212	35.2	0.9987
	6	0.002 293	0.004 943	0.2475	35.4	0.9971
	7	0.002 414	0.004 601	0.2785	35.4	0.9895
0.5	2	0.001 654	0.004 949	0.2050	34.5	0.9724
	3	0.001 865	0.004 803	0.2407	34.8	0.9936
	4	0.002 006	0.004 503	0.1437	34.4	0.9867
	7	0.002 407	0.005 611	0.2165	36.8	0.9924
0.05	2	0.001 818	0.007 473	0.1811	23.5	0.9993
	4	0.002 238	0.008 700	0.2021	24.5	0.9910
	7	0.002 681	0.011 52	0.2164	23.1	0.9788

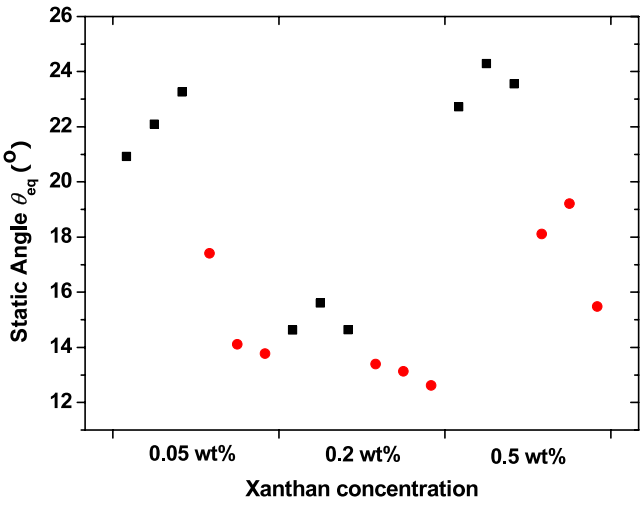

Figure 5. Static contact angles for xanthan solutions on glass. Black squares, 3 μl for 0.2 wt% and 6 μl for 0.05 and 0.5 wt%; red dots, 0.5 μl.

the droplet would spread faster. This observation correlates qualitatively with the model by Starov *et al* [9] in the case of complete wetting and small dynamic contact angle. Effects of droplet volume were not explicitly revealed in the form of equation (18).

Static contact angle (θ_0) is an essential parameter determining the spreading dynamics of partial wetting fluids. Spreading tests with droplet relaxation commonly adopted small droplets to exclude the gravity effects [11, 13, 14].

The present tests revealed that the droplet volume affects the static contact angle (figure 5). Hence, the possible role of gravity may not be totally negligible for the reported non-Newtonian fluid tests.

3.5. Dynamic contact angle and spreading velocity

When the contact line moves, the dynamic contact angle (θ) would deviate from the static contact angle (θ_{eq}) to yield the driving energy from the non-compensated surface tension force (equation (12)). Meanwhile, the shear force confronts the movement of the contact line. Under the steady spreading condition, the viscous dissipation is balanced with the driving energy (equation (11)), and produces the following equation for Newtonian fluids [7].

$$\log(\cos\theta_{eq} - \cos\theta) = \log\left(\frac{U}{\theta}\right) + \log\left(\frac{3\mu\varsigma}{\sigma}\right) \tag{19}$$

where ς is the logarithm of the ratio of the macroscopic size to a microscopic cutoff length.

Carré and Eustache [7] assumed a liquid wedge at the contact line and deduced the velocity distribution of the wedge and obtained the viscous dissipation as follows:

$$E_v = \int_{\text{liquid}} \tau \frac{\partial v}{\partial z}\,dx\,dy = \int_{x_m}^{R}\int_0^h a\left(\frac{\partial v}{\partial z}\right)^{n+1} dz\,dx$$
$$= a\frac{(2n+1)^n}{(1-n)(n\theta)^n}U^{n+1}(R^{1-n} - x_m^{1-n}). \tag{20}$$

Around the microscopic cutoff length, x_m, the liquid wedge is curved by long-range van der Waals forces. Carré and Eustache limited their discussions with shear-thinning fluids ($n < 1$), hence $x_m^{1-n} \ll R^{1-n}$ and is removed from the final expression of the relationship between θ and U:

$$\log(\cos\theta_{eq} - \cos\theta) = n\log\left(\frac{U}{\theta}\right) + \log\left(\frac{\phi k}{\sigma}\right), \qquad n < 1 \tag{21}$$

where $\phi = R^{1-n}\frac{(2+\frac{1}{n})^n}{1-n}$. Notably, equation (21) is similar in form to the Newtonian case (equation (19)). Carré and Eustache [7] noted linear correlation for their spreading data with PDMS + silica and acrylic typographic ink in $\log(\cos\theta_{eq} - \theta)$–$\log(U/\theta)$ scales with the slope denoting the corresponding power exponent n.

Equation (21) fails to describe the spreading of shear-thickening fluids since it acquires $x_m \gg R$ for avoiding the divergence in energy dissipation at the cutoff length. This contracts the assumption that the cutoff length presents an incremental distance from the contact line to prevent the stress singularity. Additionally, fitting data by Carré and Eustache [7] using equation (21) yields $R = 0.529$ and 9.804 μm for PDMS + silica and ink tests, respectively. The fit R values for shear-thinning fluids are unrealistic.

Neogi and Ybarra [54] investigated spreading dynamics using Ellis fluids and Reiner–Rivlin fluids in a capillary spreading regime. They also adopted the lubrication approximation and energy balance method as in [7]. Taking limits at the dimensionless $H \to 0$ and at $H \to \infty$ yields an approximate expression for Ellis (shear-thinning) fluids as follows:

$$E_v = \frac{3\mu_0 U^2}{\theta} \ln L - (\alpha+2)^{1/\alpha} \frac{3\mu_0 U}{\theta^{1/\alpha}} \left(\frac{x_m}{h_0}\right)^{1-1/\alpha} \tag{22}$$

where $h_0 = 3\mu_0 U/\tau_{1/2}$ and L is the macroscopic characteristic dimension of the wetting system. Since x_m is small and $\alpha > 1$, the second term on the right-hand side is negligible. Then the dissipation is almost the same as that of Newtonian fluids [1]:

$$E_v \sim \frac{3\mu U^2}{\theta} \ln\left(\frac{L}{l}\right) \tag{23}$$

where l is the microscopic cutoff length of the magnitude of molecular dimensions, and should depend on the removal formulation of the stress singularity. Therefore, Neogi and Ybarra proposed that Newtonian results would hold for Ellis fluids by the substitution of zero shear viscosity μ_0 for the constant viscosity.

The conclusion by Neogi and Ybarra is incompatible with analysis by Carré and Eustache [7] and with the experimental results [7, 13]. Arguments may arise from the physical interpretation of characteristic length L. Restated, if L is comparable to x_m, the second term in equation (22) may have an effect on the spreading. As mentioned above, the data fitting based on Carré and Eustache's data reveal that L (that is, R) is of the order of 10^{-5}–10^{-6} m. The conclusions made by Neogi and Ybarra should be revisited to resolve this controversy.

Starov *et al* [9] deduced the analytical solution for the droplet profile of spreading power-law fluids in the gravity regime. However, for the capillary wetting regime, no analytical solution was available for the dimensionless equation of droplet thickness stated in the following:

$$\left(\frac{1}{\hat{r}^m}(\hat{r}^m \zeta')'\right)' = \mathrm{sgn}\lambda |\lambda|^n \zeta^{-n-1} \tag{24}$$

where λ is a dimensionless constant and $\hat{r} = r/R(t)$. Starov *et al* [9] proposed that the part of complete wetting power-law fluid droplets that controls spreading is the spherical cap except in a limited region near the contact line; hence, the right-hand term in equation (24) is negligible and the dynamic contact angle equation in the capillary wetting regime can be stated as follows:

$$\theta \approx \tan\theta = 8\left(\frac{2n+1}{\lambda}\right)^{\frac{3n}{7+2n}} \left(\frac{V}{2\pi}\right)^{\frac{1-n}{7+2n}} \left(\frac{kU}{\sigma}\right)^{\frac{3}{7+2n}}. \tag{25}$$

The theoretical analyses by Carré and Eustache [7], Wang *et al* [13] and numerical analysis by Betelu and Fontelos [8, 10] all demonstrated a non-spherical droplet shape on spreading. The theories by Carré and Eustache [7] and Wang *et al* [13] revealed that the local film thickness is proportional to $x^{3/(n+2)}$ (distance from contact line) for shear-thinning fluids in capillary spreading. Deviation from spherical shape increases with increasing n index. For instance, $h(x) \sim x^{1.08}$ for PDMD + silica spreading [7], and $h(x) \sim x^{1.35-1.40}$ for xanthan solutions [14].

Wang *et al* [13] analyzed the evolution equation for liquid film thickness with the lubrication approximation and derived the dynamic contact angle expressions for power-law fluids in complete wetting spreading:

$$\theta_D \approx tg\theta_D = \left(\frac{k}{\sigma}U^n\right)^{\frac{1}{n+2}} \left(\frac{3^{n+1}(n+2)^{1-n}}{(2n+1)^{1-n}(1-n)n^n}\right)^{\frac{1}{n+2}} \times x_m^{\frac{1-n}{n+2}} \qquad n < 1 \tag{26a}$$

$$\theta_D \approx tg\theta_D = \left(\frac{k}{\sigma}U^n\right)^{\frac{1}{n+2}} \left(\frac{3^{n+1}(n+2)^{1-n}}{(2n+1)^{1-n}(n-1)n^n}\right)^{\frac{1}{n+2}} \times x_m^{\frac{1-n}{n+2}} \qquad n > 1 \tag{26b}$$

where x_m is the cutoff length. These authors adopted the 'shift factor' concept proposed by Hoffman [58] to extend these equations to partial wetting fluids. The generalized expressions of dynamic contact angle were obtained as follows:

$$\cos\theta_0 - \cos\theta = \frac{1}{2}\left(\frac{k}{\sigma}U^n\right)^{\frac{2}{n+2}} \left(\frac{3^{n+1}(2n+1)^{n-1}}{(n+2)^{n-1}(1-n)n^n}\right)^{\frac{2}{n+2}} \times x_m^{2\frac{1-n}{n+2}} \qquad n < 1 \tag{27a}$$

$$\cos\theta_0 - \cos\theta = \frac{1}{2}\left(\frac{k}{\sigma}U^n\right)^{\frac{2}{n+2}} \left(\frac{3^{n+1}(2n+1)^{n-1}}{(n+2)^{n-1}(n-1)n^n}\right)^{\frac{2}{n+2}} \times x_m^{2\frac{1-n}{n+2}} \qquad n > 1. \tag{27b}$$

Wang *et al* [13] correlate well the proposed equations (26) and (27) with the wetting data for both shear-thinning and shear-thickening fluids on completely or partially wetting substrates. Efforts are to be made to make clear why one can extend the use of equations (26)–(27).

3.6. Extension of Newtonian fluid models to power-law fluids and perspectives

As discussed in section 2, there are at least five approaches for relieving the stress singularity difficulty in modeling. However, as shown in figure 2, the prevailing models for non-Newtonian fluids solve the Navier–Stokes equations with shear-thinning conditions at the contact line. These models correlate limited experiment data, leaving some non-trivial problems unresolved. The use of other spreading models on power-law fluids are herein discussed.

In complete wetting tests, precursor films may also exist in front of the non-Newtonian fluid droplets (figure 1(a), lower panel). The solution procedures will resemble those with Newtonian fluids, but with different matching functions incorporating the solutions between precursor film and the external flow which turns in non-Newtonian types. The thickness of precursor films for non-Newtonian fluids can be applied for matching the bulk flow solution, such as $h(x_m)$ in Carré's model. Additionally, the energy dissipation in the non-Newtonian precursor film can be used in formulating the total energy balance for the spreading droplets.

Various slip boundary conditions can also be imposed on non-Newtonian fluid spreading modeling (figure 1(b), lower panel). However, the mathematical implementation would be quite lengthy by adopting a complex constitutive expression for non-Newtonian fluids. The no-slip boundary conditions in the available models for non-Newtonian droplet spreading can be replaced. This approach should be particularly useful for modeling shear-thickening fluid spreading.

The shear-thinning hypothesis proposed by [34–36] will work equally well in the shear-thinning fluids (figure 1(c), lower panel). As discussed in section 3.3, the shear-thickening fluid may reveal a flow characteristic similar to those with an $n_{\text{app}} < n$. As hypothesized in section 3.3, the limited mass transfer rate of dispersed silica particles in the PEG suspension to the contact line regime may be contribute to the noted decreased n_{app} in tests. Hence, the shear-thinning hypothesis may interpret the spreading of shear-thickening fluids if the local rheological properties are altered by the applied fluid fields.

The diffuse-interface model is a promising way for handling divergent dissipation at the contact line (figure 1(d), lower panel). The model generally involves modified Navier–Stokes equations associated with the microscopic structure of the interface [42]. To minimize the dissipation, let the variables $\alpha_1, \alpha_2, \ldots \alpha_i$ describe the displacement from thermodynamic equilibrium; the variational principle can be applied as follows [41]:

$$\delta[\Phi(\dot{\alpha}, \dot{\alpha}) + \dot{F}(\dot{\alpha}, \dot{\alpha})] = \sum_{i=1}^{n} \left(\frac{\partial \Phi}{\partial \dot{\alpha}_i} + \frac{\partial F}{\partial \alpha_i} \right) \delta \dot{\alpha}_i = 0 \quad (28)$$

where $\Phi(\dot{\alpha}, \dot{\alpha})$ is the dissipation function and $\dot{F}(\dot{\alpha}, \dot{\alpha})$ is the rate of change of the free energy. The free energy is assumed to be composed of a Landau free energy functional and the interfacial free energy per unit area at the fluid–solid interface. Then the dissipation function $\Phi(\dot{\alpha}, \dot{\alpha})$ for immiscible two-phase flows can be formulated considering various forms of dissipation. The hydrodynamic model for the contact line motion can be formulated by solving equation (28), supplemented with the incompressibility condition $\nabla \cdot v = 0$. Equation (28) can be formulated based on non-Newtonian fluid rheology considering the dissipation expression. Detailed derivation and analysis is worthy of further investigation.

The MKT revealed a dynamic contact angle that is independent of liquid viscosity [46, 47]; therefore, the spreading of Newtonian and non-Newtonian liquids should be handled in a similar way. The MKT was further extended to consider the effects of apparent viscosity [47], equilibrium contact angle and reversible work of adhesion [48]. The correlation between dynamic contact angle and spreading speed in MKT is described as

$$\cos\theta = \cos\theta_{\text{eq}} - \frac{2kT}{\sigma\lambda^2} \operatorname{arcsin} h\left(\frac{V}{2K_{\text{w}}\lambda} \right) \quad (29)$$

where k is Boltzmann's constant, T is the temperature, λ is the typical distance between two neighboring absorption sites on the solid surface, and K_w is the equilibrium frequency resulting from molecular displacements in the direction of spreading. K_w is related to the activation free energy of wetting ΔG_0 by

$$K_{\text{w}} = \frac{kT}{h} \exp\left(-\frac{\Delta G_0}{NkT} \right) \quad (30)$$

where h is Planck's constant and N is Avogadro's number.

Compared with the exhaustive studies on Newtonian fluid spreading, the available theoretical models for non-Newtonian liquid spreading are rather limited. Very different forms of constitutive equations for fluid rheology are presented for typical non-Newtonian fluids. Competition among various forces acting at the contact line regime for numerous kinds of non-Newtonian fluids deserves detailed discussion.

Acknowledgment

This study was supported by the National Natural Science Foundation of China (No 50636020).

Appendix. Experimental section

A.1. Samples

All chemicals were of highest purity from Sigma-Aldrich (Taiwan) and were used without further purification. Xanthan solutions were the test samples. Xanthan solutions on a mica surface present complete wetting, while the xanthan solutions on a glass slide are partial wetting systems.

A clean microscope glass slide and mica were the tested solid substrates. For the microscope glass slide all experiments were conducted on the same piece of the slide and the slide was cleaned strictly using detergent, ultra-pure water, 99.5% ethanol, 2N nitric acid, and acetone, with ultrasonication. The mica foils were split carefully to get clean and smooth surfaces. Before each experiment dry nitrogen was flowed to dry the slide or mica.

A.2. Measurements and tests

The surface tensions of all tested liquids were measured by a Krúss Processor Tensiometer K12 (Krúss GmbH, Hamburg, Germany). A cone-plate rheometer (Advanced Rheometric Expansion System) measured the apparent viscosity versus shear rate relationship for all tested liquids.

The static contact angle and the drop spreading dynamics tests were conducted using an FTA125 Dynamic Contact Angle Analyzer (Contact Angle and Surface Tension Instruments, Portsmouth, USA). A drop of selected liquid of volume 0.5–7 μl was deposited from the top of the horizontally placed substrate. The measurement results are listed in table A.1.

The images of the deposited drop were recorded at 60 frames s^{-1} by a CCD camera and sent to a computer for storage and processing. The contact angle $\theta(t)$ and the wetting radius $R(t)$ as function of time t were obtained by analyzing each frame with the built-in software using non-spherical fitting. The static contact angle was measured at the end of the spreading test. At least four identical tests were

Table A.1. Characteristics of fluids tested in the present work.

Concentration of xanthan (ppm)	Stable σ (mN m^{-1})	k (Pa s^n)	n	l_c (mm)	Volume (μl)	Substrate	Note
500	65.93	0.032 96	0.6292	2.59	2/4/7	Glass slide	Tested at 28 °C
5 000	49.90	3.529	0.2260	2.26	2/3/4/7	Glass slide	
10 000	43.55	7.990	0.1930	2.11	2–7	Glass slide	
500	72.81	0.0644	0.5973	2.73	0.5/6	Glass slide	Tested at 20 °C
					0.5/3	Mica	
2 000	68.97	0.6468	0.3816	2.65	0.5/3	Glass slide	
					0.5/3	Mica	
5 000	57.17	4.409	0.2093	2.42	0.5/6	Glass slide	
					0.5/3	Mica	

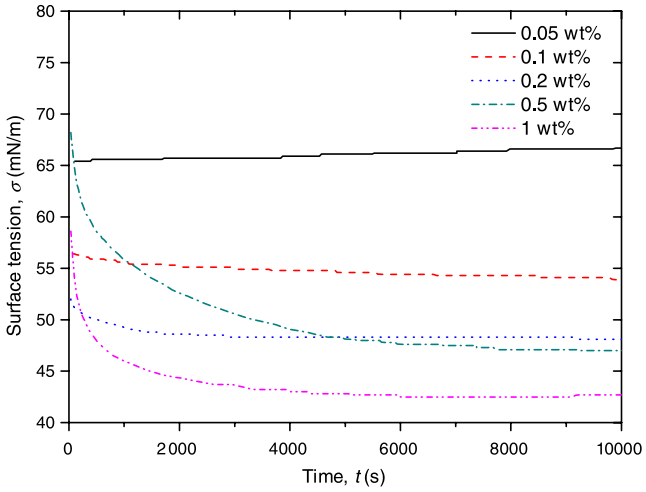

Figure A.1. Surface tension tests of xanthan solutions.

conducted under each experimental condition to assure data reproducibility.

The test xanthan solutions have capillary length of 2.2–2.6 mm. Hence, the drop radius range covered the capillary and gravitational spreading regimes.

A.3. Surface tension measurements

The surface tensions of xanthan solution present the most widely used shear-thinning fluid tested in the literature [11, 13, 14, 55]. However, its reported surface tension data revealed discrepancy. For instance, surface tension of xanthan solutions was reported in a range of 44–66 mN m^{-1} [14], at a constant of 72 mN m^{-1} at 20 °C [11], or of 65 mN m^{-1} at 25 °C [55]. We tested herein and noted dynamic surface tension (DST) effects (figure A.1). Preparation and handling of xanthan solutions before spreading tests could affect the experimental results.

References

[1] de Gennes P G 1985 Wetting: statics and dynamics *Rev. Mod. Phys.* **57** 827–63
[2] Leger L and Joanny J F 1992 Liquid spreading *Rep. Prog. Phys.* **55** 431–86
[3] Voinov O V 2002 *Encyclopedia of Surface and Colloid Science* ed A T Hubbard (New York: Dekker) pp 1546–59
[4] Blake T D 2006 The physics of moving wetting lines *J. Colloid Interface Sci.* **299** 1–13
[5] de Gennes P G, Brochard-Wyart F and Quéré D 2004 *Capillarity and Wetting Phenomena: Drops, Bubbles, Pearls, Waves* (New York: Springer)
[6] Starov V M, Velarde M G and Radke C J 2007 *Wetting and Spreading Dynamics* (Boca Raton, FL: CRC Press)
[7] Carré A and Eustache F 2000 Spreading kinetics of shear-thinning fluids in wetting and dewetting modes *Langmuir* **16** 2936–41
[8] Betelu S I and Fontelos M A 2003 Capillarity driven spreading of power-law fluids *Appl. Math. Lett.* **16** 1315–20
[9] Starov V M, Tyatyushkin A N, Velarde M G and Zhdanov S A 2003 Spreading of non-Newtonian liquids over solid substrates *J. Colloid Interface Sci.* **257** 284–90
[10] Betelu S I and Fontelos M A 2004 Capillarity driven spreading of circular drops of shear-thinning fluid *Math. Comput. Modelling* **40** 729–34
[11] Rafai S, Bonn D and Boudaoud A 2004 Spreading of non-Newtonian fluids on hydrophilic surfaces *J. Fluid Mech.* **513** 77–85
[12] Rafai S and Bonn D 2005 Spreading of non-Newtonian fluids and surfactant solutions on solid surfaces *Physica* A **358** 58–67
[13] Wang X D, Lee D J, Peng X F and Lai J Y 2007 Spreading dynamics and dynamic contact angle of non-Newtonian fluids *Langmuir* **23** 8042–7
[14] Wang X D, Zhang Y, Lee D J and Peng X F 2007 Spreading of completely wetting or partially wetting power-law fluid on solid surface *Langmuir* **23** 9258–62
[15] Ogarev V A, Timonina T N, Arslanov V V and Trapezni A A 1974 Spreading of polydimethylsiloxane drops on solid Horizontal surfaces *J. Adhes.* **6** 337–55
[16] Tanner L H 1979 Spreading of silicone oil drops on horizontal surfaces *J. Phys. D: Appl. Phys.* **12** 1473
[17] Lopez J, Miller C A and Ruckenstein E 1976 Spreading kinetics of liquid-drops on solids *J. Colloid Interface Sci.* **56** 460–8
[18] Cazabat A M and Stuart M A C 1986 Dynamics of wetting: effects of surface-roughness *J. Phys. Chem.* **90** 5845–9
[19] Ehrhard P 1993 Experiments on isothermal and non-isothermal spreading *J. Fluid Mech.* **257** 463–83
[20] Biance A L, Clanet C and Quere D 2004 First steps in the spreading of a liquid droplet *Phys. Rev.* E **69** 016301
[21] Kavehpour P, Ovryn B and McKinley G H 2002 Evaporatively-driven Marangoni instabilities of volatile liquid films spreading on thermally conductive substrates *Colloids Surf.* A **206** 409–23
[22] Lavi B and Marmur A 2004 The exponential power law: partial wetting kinetics and dynamic contact angles *Colloids Surf.* A **250** 409–14

[23] Huh C and Scriven L E 1971 Hydrodynamic model of steady movement of a solid/liquid/fluid contact line *J. Colloid Interface Sci.* **35** 85–101
[24] Hervet H and de Gennes P G 1984 The dynamics of wetting: precursor films in the wetting of dry solids *C. R. Acad. Sci., Paris* II **299** 499–503
[25] Joanny J F and de Gennes P G 1984 Competition between wetting and adverse macroscopic forces *C. R. Acad. Sci., Paris* II **299** 605–8
[26] Ausserre D, Picard A M and Leger L 1986 Existence and role of the precursor film in the spreading of polymer liquids *Phys. Rev. Lett.* **57** 2671–4
[27] Beaglehole D 1989 Profiles of the precursor of spreading drops of siloxane oil on glass, fused-silica, and mica *J. Phys. Chem.* **93** 893–9
[28] Kavehpour H P, Ovryn B and McKinley G H 2003 Microscopic and macroscopic structure of the precursor layer in spreading viscous drops *Phys. Rev. Lett.* **91** 196104
[29] Voinov O V 1976 Hydrodynamics of wetting *Fluid Dyn.* **11** 714–21
[30] Cox R G 1986 The dynamics of the spreading of liquids on a solid surface. I. Viscous flow *J. Fluid Mech.* **168** 169–94
[31] Koplik J, Banavar J R and Willemsen J F 1989 Molecular dynamics of fluid flow at solid surfaces *Phys. Fluids* A **1** 781–94
[32] Thompson P A and Robbins M O 1989 Simulations of contact-line motion: slip and the dynamic contact angle *Phys. Rev. Lett.* **63** 766–9
[33] Thompson P A and Troian S M 1997 A general boundary condition for liquid flow at solid surfaces *Nature* **389** 360–2
[34] Weidner D E and Schwartz L W 1994 Contact-line motion of shear-thinning liquids *Phys. Fluids* **6** 3535–8
[35] Ansini L and Giacomelli L 2002 Shear-thinning liquid films: macroscopic and asymptotic behaviour by quasi-self-similar solutions *Nonlinearity* **15** 2147–64
[36] Carre A and Woehl P 2006 Spreading of silicone oils on glass in two geometries *Langmuir* **22** 134–9
[37] Seppecher P 1996 Moving contact lines in the Cahn-Hilliard theory *Int. J. Eng. Sci.* **34** 977–92
[38] Jacqmin D 2000 Contact-line dynamics of a diffuse fluid interface *J. Fluid Mech.* **402** 57–88
[39] Pismen L M and Pomeau Y 2000 Disjoining potential and spreading of thin liquid layers in the diffuse-interface model coupled to hydrodynamics *Phys. Rev.* E **62** 2480–92
[40] Pomeau Y 2002 Recent progress in the moving contact line problem: a review *C. R. Mec.* **330** 207–22
[41] Qian T Z, Wang X P and Sheng P 2006 A variational approach to moving contact line hydrodynamics *J. Fluid Mech.* **564** 333–60
[42] Khatavkar V V, Anderson P D and Meijer H E H 2007 Capillary spreading of a droplet in the partially wetting regime using a diffuse-interface model *J. Fluid Mech.* **572** 367–87
[43] Shikhmurzaev Y D 1993 The moving contact line on a smooth solid surface *Int. J. Multiph. Flow* **19** 589–610
[44] Shikhmurzaev Y D 1994 Mathematical modeling of wetting hydrodynamics *Fluid Dyn. Res.* **13** 45–64
[45] Shikhmurzaev Y D 1997 Moving contact lines in liquid/liquid/solid systems *J. Fluid Mech.* **334** 211–49
[46] Blake T D and Haynes J M 1969 Kinetics of liquid/liquid displacement *J. Colloid Interface Sci.* **30** 421
[47] Blake T D 1993 *Wettability* ed J C Berg (New York: Dekker) pp 251–309
[48] Blake T D and De Coninck J 2002 The influence of solid–liquid interactions on dynamic wetting *Adv. Colloid Interface Sci.* **96** 21–36
[49] Glasstone S, Laidler K J and Eyring H 1941 *The Theory of Rate Processes* (New York: McGraw-Hill)
[50] Cox R G 1998 Inertial and viscous effects on dynamic contact angles *J. Fluid Mech.* **357** 249–78
[51] Stoev K, Rame E and Garoff S 1999 Effects of inertia on the hydrodynamics near moving contact lines *Phys. Fluids* **11** 3209–16
[52] Hocking L M and Davis S H 2002 Inertial effects in time-dependent motion of thin films and drops *J. Fluid Mech.* **467** 1–17
[53] Nieh S Y, Ybarra R M and Neogi P 1996 Wetting kinetics of polymer solutions. Experimental observations *Macromolecules* **29** 320–5
[54] Neogi P and Ybarra R M 2001 The absence of a rheological effect on the spreading of small drops *J. Chem. Phys.* **115** 7811–3
[55] Seevaratnam G K, Suo Y, Rame E, Walker L M and Garoff S 2007 Dynamic wetting of shear thinning fluids *Phys. Fluids* **19** 012103
[56] Boudaoud A 2007 Non-Newtonian thin films with normal stresses: dynamics and spreading *Eur. Phys. J.* E **22** 107–9
[57] de Ruijter M J, de Coninck J and Oshanin G 1999 Droplet spreading: partial wetting regime revisited *Langmuir* **15** 2209–16
[58] Hoffman R L 1975 Study of advancing interface. 1. Interface shape in liquid–gas systems *J. Colloid Interface Sci.* **50** 228–41